



# A methodology for expanding the use of NaI(Tl) based spectrometry in environmental radioactivity measurements

M. Pilakouta<sup>a,\*</sup>, F.K. Pappa<sup>b,d</sup>, D.L. Patiris<sup>b</sup>, C. Tsabaris<sup>b</sup>, C.A. Kalfas<sup>c</sup>

<sup>a</sup> Automation Engineering Department, Piraeus University of Applied Sciences (TEI of Piraeus), Petrou Ralli & Thivon 250, Aegaleo, Athens 12244 Greece

<sup>b</sup> Institute of Oceanography, Hellenic Centre for Marine Research, Anavyssos, Attiki 19013, Greece

<sup>c</sup> National Centre for Scientific Research Demokritos, Institute of Nuclear & Particle Physics, 15310 Agia Paraskevi, Greece

<sup>d</sup> Department of Physics, National Technical University of Athens, Zografou, Athens 15780, Greece

## HIGHLIGHTS

- A methodology of exploiting the use of NaI(Tl) detectors in environmental research.
- Utilizing low resolution  $\gamma$ -ray detectors in radiation protection.
- Improved uranium and thorium concentration measurements in building materials.

## ARTICLE INFO

### Keywords:

Gamma ray Spectroscopy  
NaI(Tl)  
Radioactivity  
Sample analysis  
Granite

## ABSTRACT

A methodology that extends the usability of low and medium resolution  $\gamma$ -ray detectors to a wide range of energies that appear in environmental radioactivity measurements is described. Results of the implementation of the methodology in the analysis of 20 granite samples measured with a (3"  $\times$  3") NaI(Tl) are presented. A comparison with the activity results obtained by a high-resolution detector (HPGe) for two samples was found in good agreement, within the uncertainties, validating the results of the proposed method.

## 1. Introduction

NaI (Tl) detectors became commercially available in the 50's and are virtually the first solid state detectors used for  $\gamma$ -ray spectrometry. Although the advances in  $\gamma$ -ray spectroscopy instrumentation has led to high resolution detectors like HPGe, NaI (Tl) detectors despite their low resolution are still available for environmental research applications. Such applications include environmental radioactivity field measurements (Tsabaris et al., 2008; Bezuidenhout, 2013; Chiozzi et al., 2003; Cinelli et al., 2016), applications in education (Pilakouta et al., 2017; Anjos et al., 2003) and in cases where the resolution is not an important issue. The main advantages of NaI (Tl) detectors are high sensitivity, low cost, low power consumption and non-cooling operation, while the main disadvantages are the low resolution, the gain drift due to changes in the ambient temperature and the nonlinearity issue. A solution to the gain drift is to use a stabilizer and/or collect spectra at short acquisition time and then sum them after recalibration, using appropriate software to acquire the total spectrum. A combination of the above methods, as in the present study, can yield better result. To minimize the non-linearity problem, the applied voltage is set to the maximum

recommended value.

In this work, a methodology is proposed to overcome the issue of low resolution. This methodology combines improved tools of software technology (Kalfas et al., 2016) with  $\gamma$ -ray data and simple equations in an attempt to de-convolute multiple peaks. Such a methodology may extend the usability of low and medium resolution  $\gamma$ -ray detectors to a wider range of energies that appear in environmental radioactivity measurements.

The  $\gamma$ -ray peaks that are typically utilized for quantitative analysis in environmental radioactivity measurements using NaI (Tl) detectors are 1460.8 keV of  $^{40}\text{K}$ , 2614.5 keV of  $^{208}\text{Tl}$  ( $^{232}\text{Th}$  decay chain) and 1764.5 keV of  $^{214}\text{Bi}$  ( $^{238}\text{U}$  decay chain) (IAEA, 2003). On the other hand, using a high resolution HPGe detector, more than 40 potential peaks can be analyzed for the specific activity determination of the  $^{232}\text{Th}$  and  $^{238}\text{U}$  chain, as shown in Table 2. In the present work the term specific activity as defined in (IUPAC, 1996; IAEA, 2016 p. 12) - and is widely understood - is used for the activity of a sample due to an isotope R: "For a specified isotope, or mixture of isotopes, the activity of a material divided by the mass of the material". For short in the rest of the article the term "activity" means the activity per unit mass of a

\* Corresponding author.

E-mail address: [mpilak@puas.gr](mailto:mpilak@puas.gr) (M. Pilakouta).

sample.

The data analysis methodology described in this work can apply successfully in environmental research using low energy resolution detectors such as NaI. It is to a considerable degree reliable and meets the needs of small laboratories where the high cost of HPGe detectors renders them unattainable and for data acquisition in environments where HPGe detectors cannot be used.

## 2. Material and methods

### 2.1. Experimental set up and samples preparation

#### 2.1.1. $\gamma$ -ray spectrometry experimental setup

The acquisition of the energy spectra from granites samples was accomplished using a  $\gamma$ -ray spectrometry system of the Piraeus University of Applied Science based on a 3"  $\times$  3" NaI detector with 7% nominal energy resolution at 662 keV. For the measurements the DigiBASE (Ortec) multi-channel analyzer and the MAESTRO multi-channel analyzer (MCA) emulation software were used for data acquisition, storage and display of the acquired  $\gamma$ -ray spectra. The detector was shielded with 5 cm thick lead-blocks to reduce the laboratory ambient background gamma radiation (BGR). The DigiBASE-E gain stabilizer was used for auto-compensation of voltage output, monitoring the centroid of 1461 keV peak in each case. Furthermore, to avoid any significant spectrum drift, spectra were registered every 2 h for a 24 h period and then the incremental spectra were recalibrated and added offline using the SPECTRW spectrum analysis software (Kalfas et al., 2016). Additionally, as reference for the test cases, spectra of the same granite samples were obtained using the high-resolution HPGe spectrometry system of the Hellenic Centre for Marine Research (Tsabaris et al., 2007) with relative efficiency 50% and 1.8 keV nominal resolution at 1332 keV.

#### 2.1.2. Samples

Samples of commercially available granites from a variety of places of origin and with 49 cm<sup>2</sup> surface, 2 cm thickness and 0.25 kg average weight, without any scratches were used for the measurements. Each sample was placed in contact with the detector in the shielded area and counted over a period of 24 h. Furthermore, a 24-h spectrum of the ambient background radiation was recorded every two days under the same conditions (experimental setup, shielding etc.) with the granite samples. The background spectrum was subtracted from that of each granite in order to get the net spectrum for further analysis.

#### 2.1.3. Efficiency calibration

The detector efficiency curve is shown in Fig. 1 and was obtained using a) a multiple  $\gamma$ -ray emitting large volume source (<sup>241</sup>Am, <sup>137</sup>Cs, <sup>60</sup>Co, <sup>210</sup>Pb) supplied by the Greek Atomic Energy Commission and separately b) a <sup>40</sup>K source. The latter was prepared in the Chemistry laboratory of the Piraeus University of Applied Sciences from KCl salt, after drying it for 24 h at 110 °C. A plastic container of dimensions 7 cm  $\times$  7 cm  $\times$  2 cm, similar in size to the granite samples, was filled with the dried salt and the net weight of the salt was obtained. To reproduce the full energy photo-peak efficiency (the term efficiency will be used) along the detector's energy range (up to 3000 keV), a 4 parameter (A, b, C, d) function (Kalfas et al., 2016) was used to fit the experimentally obtained results:

$$\text{Efficiency} = \frac{A \text{ Energy}^b}{1000 C + \text{Energy}^d} \quad (1)$$

It should be noted that in a low-resolution detector, a <sup>152</sup>Eu source (traditionally used for HPGe efficiency calibration) with its many photo-peaks, most of which cannot be resolved, is not so suitable. However, if such a source is available, it can serve to check the validity of the efficiency curve in the region 100–400 keV since the first three

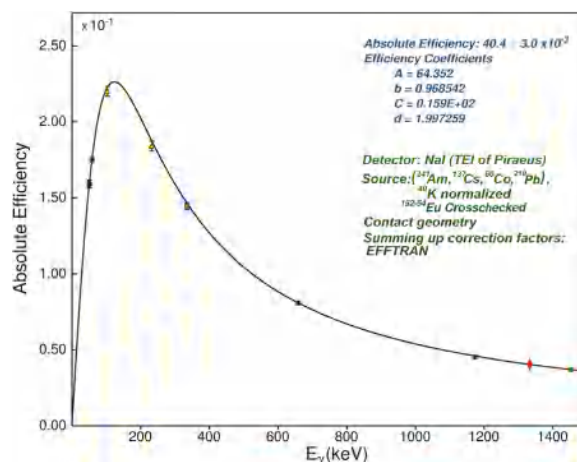


Fig. 1.: Efficiency Calibration curve of the 3"  $\times$  3" NaI in contact geometry. The uncertainty bars corresponds to 95% confidence level.

major photo-peaks, i.e. those at 121.8, 244.7 and 344.3 keV are clearly resolved. If the source is a mixture of <sup>152</sup>Eu and <sup>154</sup>Eu, the activity ratio of the two isotopes must be known. This verification was applied in the present work. The sources were placed in contact with the front face of the detector, in the same geometry as the samples. All the appropriate corrections were taken into account (geometry, summing corrections, self-absorption (Vidmar, 2005)).

### 2.2. Methodology of spectra analysis

In this work, a methodology is proposed to overcome the issue of low resolution spectra obtained from NaI(Tl) detectors resulting in a spectrum containing a number of "composed or convoluted peaks" each of them being a convolution of several "individual"  $\gamma$ -rays photo-peaks. In general, the activity of an isotope  $C_R$  is determined from each "individual" photo-peak of  $\gamma$ -ray from the equation:

$$C_R = S_f \frac{N_{E_\gamma}}{m t \varepsilon_{E_\gamma} I_\gamma} \quad (2)$$

where,  $N_{E_\gamma}$  is the net number of counts of the individual photo-peak,  $m$  the mass of the sample,  $t$  the real acquisition time,  $\varepsilon_{E_\gamma}$  the efficiency at the energy  $E$ ,  $I_\gamma$  the decay emission probability and  $S_f$  is the summing correction factor. If mass is in kg and time in s, the activity is in Bq/kg, while  $S_f$ ,  $\varepsilon_{E_\gamma}$  and  $I_\gamma$  are unit-less parameters. The net number of counts  $N_{E_\gamma}$  is obtained by subtracting the background counts from the total counts of the photo-peak.

In the case of a composed peak (with centroid in the energy  $E_{cy}$ ) produced by the convolution of several individual photo-peaks (each with centroid in the energy  $E_{yi}$ ), the net number of counts  $N_{E_{cy}}$  can be expressed as:

$$N_{E_{cy}} = \sum_1^n e_{E_{yi}} C_U + \sum_1^k e_{E_{yi}} C_{Th} \quad (3)$$

where,  $n$  and  $k$  are the number of "individual" photo-peaks produced by <sup>238</sup>U and <sup>232</sup>Th progenies respectively,  $C_U$  and  $C_{Th}$  the activity of <sup>238</sup>U and <sup>232</sup>Th in the sample. For each individual photo-peak  $e_{E_{yi}}$  is a short description of:

$$e_{E_{yi}} = \frac{m t \varepsilon_{E_\gamma} I_\gamma}{S_f} \quad (4)$$

Thus the activities of U and Th series can be obtained using a set of equations based on the analysis of each composed peak.

In this work, an alternative way to determine the activity from both series is proposed and demonstrated for the case of granites samples (test cases) based on the analysis of each "individual" photo-peak as well as, on new stripping methods (case of 1460 keV photo-peak). The

corresponding radionuclides of each individual photo-peak composing the convoluted peaks are identified (as well as any other interferences) and the activity of  $^{238}\text{U}$  and  $^{232}\text{Th}$  are estimated and evaluated with each “individual peak” measurements uncertainty, in the same way as in high resolution HPGe spectrometry. The spectra acquired by the HPGe detector for the same test case samples are used as references and for validation purposes.

The methodology comprises the following steps: In each energy region,  $\gamma$ -ray peaks in the NaI spectrum of the examined sample are selected (free of unknown contaminants and with a moderate or higher intensity). The expected  $\gamma$ -lines in each “wider peak” of the spectrum and the isotopes to which they belong are noted. The efficiency coefficients, emission probabilities (Firestone, 1996) and true summing correction factors (for short: summing factor) for each line (Vidmar, 2005) are necessary in order to split the total area of the wide peaks to its components, as explained below in Section 3.1 In section 3.2 the uncertainty evaluation is explained.

### 3. The proposed methodology for low resolution spectra analysis

#### 3.1. The analysis of the spectra

In this work, the activities of  $^{238}\text{U}$  and  $^{232}\text{Th}$  were obtained by measuring the corresponding activities of ( $^{214}\text{Bi}$ ,  $^{214}\text{Pb}$ ) and ( $^{208}\text{Tl}$ ,  $^{228}\text{Ac}$ ,  $^{212}\text{Pb}$ ,  $^{212}\text{Bi}$ ), as progenies of  $^{226}\text{Ra}$  and  $^{228}\text{Th}$  respectively and assuming secular equilibrium between  $^{238}\text{U}$  and  $^{232}\text{Th}$  with all their respective progenies inside the granite samples. This assumption was justified by comparing the activities of isotopes obtained by measurements with a high-resolution HPGe system as they are presented in Table 3. Two granite samples were chosen, one with relatively high activity (Test sample1: Giallo California) and one with significantly lower one (Test sample2: New Caledonia).

In order to demonstrate the methodology, the analysis of Test sample1 follows. The starting point is the most reliable photo-peak in the NaI spectrum at 2614 keV corresponding solely to  $^{208}\text{Tl}$  and being free of any neighboring peaks. The number of net counts  $N_0$  is modified using the detector efficiency at the energy  $E = 2614$  keV, the decay emission probability of  $^{208}\text{Tl}$  and the summing factor (Vidmar, 2005) through the relation:

$$N_{E_{2614}} = \frac{N_0 S_f}{\epsilon_{E_{2614}} I_\gamma} \tag{5}$$

With this modification,  $N_E$  represents the number of counts that would have been detected for 100% efficiency, 100% decay emission probability and with no summing effects.  $^{208}\text{Tl}$  has another photo-peak at 583 keV, which is convoluted with the 609 keV of the  $^{214}\text{Bi}$  (Fig. 2a). The fitting procedure serves to evaluate the net total number of counts under the composite peak, as plotted in Fig. 2b. As the activity of  $^{208}\text{Tl}$  is the same regardless which photo-peak will be analyzed, the expected number of counts for the 583 keV photo-peak can be calculated combining the modified number of counts of the 2614 keV (Eq. (5)) and applying the Eq. (2) by the relation:

$$N_{E_{583}} = \frac{N_{E_{2614}} \epsilon_{E_{583}} I_{\gamma_{583}}}{S_{f_{583}}} \tag{6}$$

where the notation is the same as in Eq. (2). The rest of the counts of the convoluted peak is then attributed to the 609 keV  $\gamma$ -ray of  $^{214}\text{Bi}$ . At this step of methodology, the measurements of  $^{214}\text{Bi}$  (609 keV) and  $^{208}\text{Tl}$  (2614 keV) number of counts can provide a first estimation of the  $^{238}\text{U}$ -chain/ $^{232}\text{Th}$ -chain activity ratio (R) by appropriately applying the Eq. (2) for both radionuclides. For this granite sample the ratio R was found approximately 0.5. According to the proposed methodology, after completing the analysis for the rest of the spectrum, this approximate value is either re-confirmed or modified if necessary, using all the activity results. In the latter case, the analysis is repeated for those photo

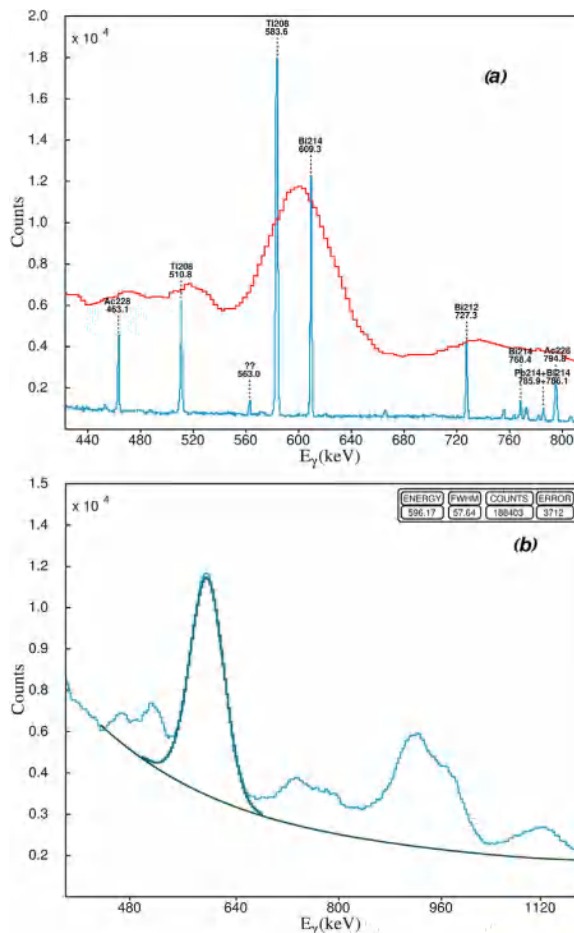


Fig. 2. (a) The HPGe and NaI spectra of the same sample in the region 420–820 keV. (b) Evaluation of the number of net counts of the 583–609 keV composite peak.

peaks that are affected by the ratio.

A very weak peak at 563.0 keV, not belonging to any of the observed isotopes in the sample, could not be identified, either as a spurious peak resulting from coincidence summing or as a single/double escape of any of the expected  $\gamma$ -lines. In any case, it has a very small contribution and can be ignored.

The next step is to divide the spectrum in 5 energy regions and analyze the composed photo-peaks contained, as described below. These regions are: a) 40–470 keV, b) 850–1000 keV, c) 1120–1380 keV, d) 1460 keV and e) 1729–1847 keV.

#### 3.1.1. Region: 40–470 keV

The peak of the 239 keV is a composed peak (Fig. 3a) produced by the convolution three  $\gamma$ -lines: i) 238.63 keV emitted from  $^{212}\text{Pb}$  with emission probability of 43.5% ii) 241.0 keV emitted from  $^{224}\text{Ra}$  with emission probability 4.05% and iii) 241.9 keV emitted from  $^{214}\text{Pb}$  with emission probability 7.46%. The efficiency coefficients are almost the same for these neighboring energies as well as, the summing factors. The estimated activity ratio of  $^{238}\text{U}$  and  $^{232}\text{Th}$  for this granite sample has been calculated based on the analysis of the 583.19 keV of  $^{208}\text{Tl}$  and 609.32 keV of  $^{214}\text{Bi}$  lines having an approximate value 0.5. This ratio (R) should be taken into account (along with the efficiency value, emission probability and summing factor) in order to determine the distribution of the counts total net counts of the convoluted peak to the three individual photo-peaks of the corresponding radionuclides belonging to different chains;  $^{214}\text{Pb}$  is progeny of  $^{238}\text{U}$  decay chain while  $^{212}\text{Pb}$  and  $^{224}\text{Ra}$  are progenies of  $^{232}\text{Th}$  decay chain. For this purpose, the distribution coefficients  $f_{E_\gamma}$  are introduced and are calculated for

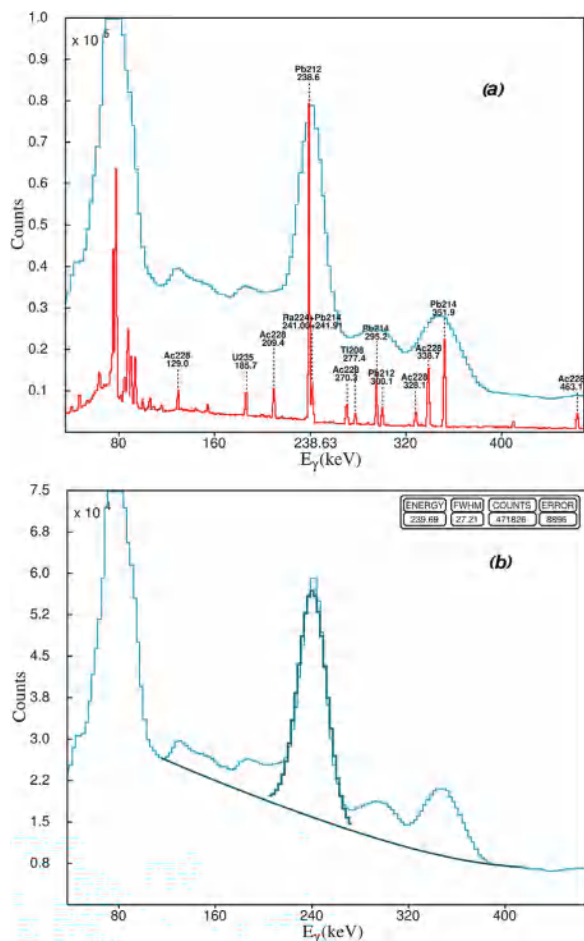


Fig. 3. (a) The HPGe and NaI spectra in the region of 40–470 keV. (b) The peak evaluation (fitting).

each involved  $\gamma$ -line using the equation:

$$f_{E_\gamma} = R \frac{\epsilon_{E_\gamma} I_\gamma}{S_f} \quad (7)$$

For the percentage expression of the distribution coefficients, for each composite peak, they are normalized to their sum so that  $\sum f_{E_\gamma} = 100$ . For this particular sample the counts of 239 keV peak is distributed as: 85% to 238 keV of  $^{212}\text{Pb}$ , 8% to 241 keV of  $^{224}\text{Ra}$  and 7% to 241.9 keV of  $^{214}\text{Pb}$ . This applies to all peak splitting to follow.

In 295 keV there is another composed peak produced by the convolution of the 295.17 keV of  $^{214}\text{Pb}$  with emission probability 19.2% and the 300.01 keV of  $^{212}\text{Pb}$  with emission probability of 3.25%. The summing up factors differs considerably so, the splitting calculation must include the different correction factors. Again the mean  $^{238}\text{U}$  and  $^{232}\text{Th}$  ratio is considered 0.5. Finally, the composed peak in 351 keV is produced by the convolution of 328.07 of  $^{228}\text{Ac}$  with emission probability 3.1%, the 338.42 of  $^{228}\text{Ac}$  with emission probability 11.26% and the 351.9 keV of  $^{214}\text{Pb}$  with emission probability 37.9%.

### 3.1.2. Region: 850–1000 keV

The expected  $\gamma$ -lines in the 911–968 keV convoluted peak (Fig. 4a) are 911.16, 964.64 and 968.97 keV of  $^{228}\text{Ac}$  and a small contribution from  $^{214}\text{Bi}$  (934.06 keV). According to the mean  $^{238}\text{U}$  and  $^{232}\text{Th}$  ratio and the procedure previously described, the total number of counts in this convoluted peak for the specific granite sample (where the ratio is 0.5) can be distributed as follows: 55.5% for the 911.16 keV, 2.6% for the 934.06 keV, 10% for the 964.64 keV and 31.9% for the 968.97 keV.

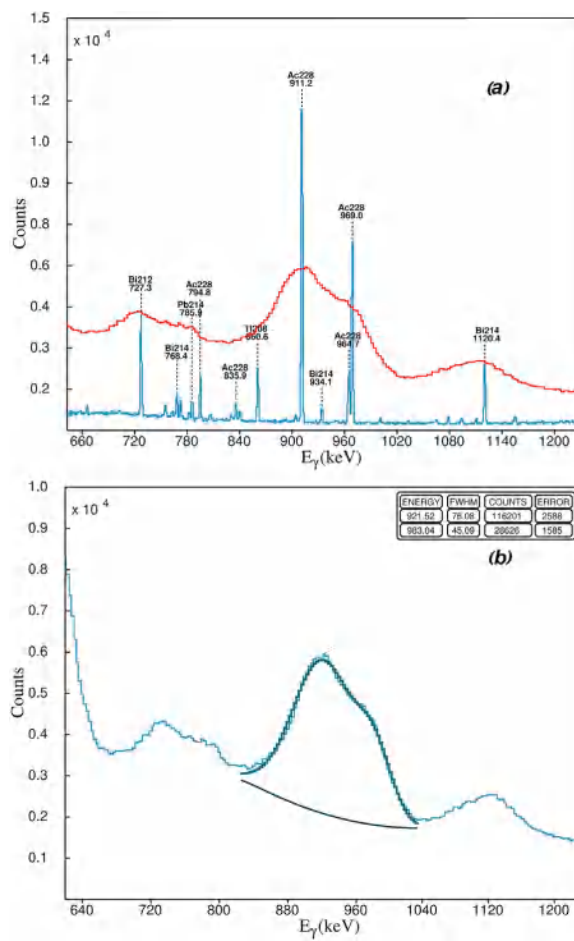


Fig. 4. (a) The HPGe and NaI spectra in the region of 850–1000 keV. (b) Deconvolution of the composite peak, evaluating the total number of counts.

### 3.1.3. Region: 1120–1380 keV

There are two major problems concerning this region. The first is the Compton-edge of the 1460.8 keV ( $^{40}\text{K}$ ) on which 3 composite peaks are superimposed. The second is the existence of 3 small photo-peaks at 1065, 1079 and 1111 keV that cannot be identified. Such peaks are often due to true coincidence summing-up. The first problem is resolved by recording a  $^{40}\text{K}$  source spectrum (under the same experimental conditions) and subtracting it after appropriate normalization in order to have the same number of counts under the photo-peak of 1460.8 keV. This will eliminate the “shoulder” of the Compton edge (Fig. 5).

The second problem is resolved with the help of the HPGe spectrum and/or the deconvolution of the composite peak in the NaI spectrum. Both gave an estimate of  $64 \pm 5\%$  for the ratio of the 1120 keV photo-peak over the total area that includes all 6 peaks (1065, 1078, 1084, 1111, 1120 and 1155 keV). Thus, the first composite peak which spans the region between 1040 and 1160 keV can split into the 1120 keV area and all the rest. The deconvolution of the other two composite peaks (Fig. 6b) is explained below.

Apart from a very small un-identifiable peak at 1245 keV (as indicated in the HPGe spectrum), the 1238 + 1281 peak in the NaI spectrum is almost free of any other interfering lines. This 1245 keV line is ignored since it is only of the order of a few per cent as compared to the sum of 1238 + 1281 keV peaks in the HPGe spectrum and in any case smaller than the experimental uncertainty in determining the area under the 1238 + 1281 composite line. As for the 1378 keV composite peak, the extra three small contributions belong to the same isotope as the 1378 keV line and the total area can split using the branching ratios, the efficiency coefficients and the summing-up factors as described

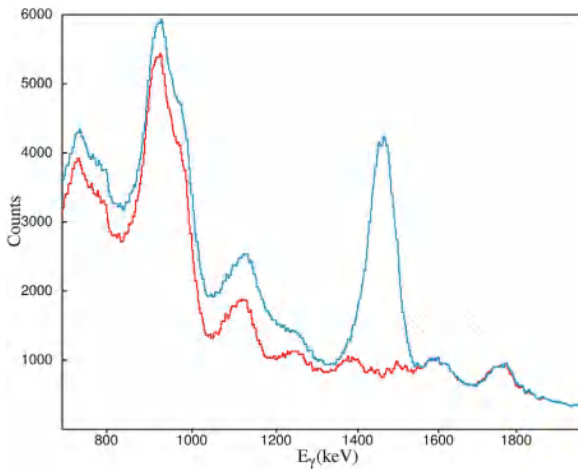


Fig. 5. Partial NaI spectrum before and after subtracting  $^{40}\text{K}$ .

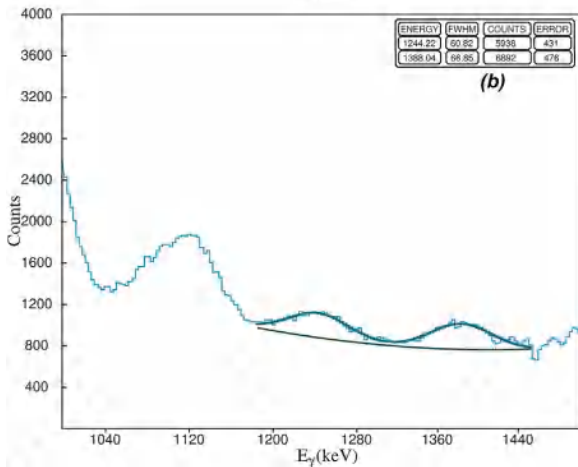
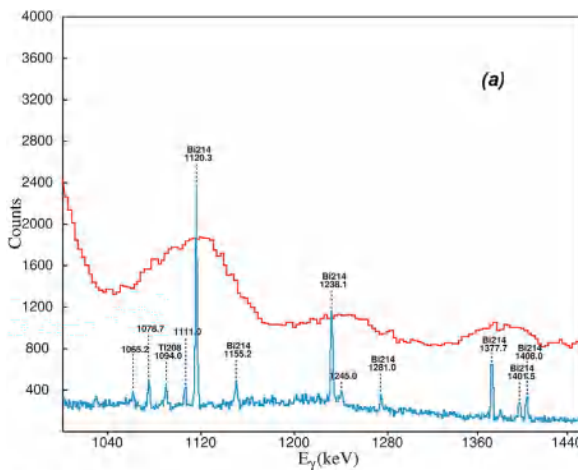


Fig. 6. (a) The HPGe and NaI spectra (after subtraction of  $^{40}\text{K}$  as shown in Fig. 5) in the region of 1120–1380 keV. (b) Evaluation of the number of net counts in the 1238 + 1281 and 1378 peaks.

before.

### 3.1.4. Region: 1460 keV

The 1460.82 keV line is almost free of any interfering peaks, as seen in the HPGe spectrum (Fig. 7a). There is only a small interfering contribution from certain  $^{214}\text{Bi}$  lines and two lines resulting from summing up effects but with negligible intensity. There are various approaches to correct for this interference. In water environment (Tsbaris et al.,

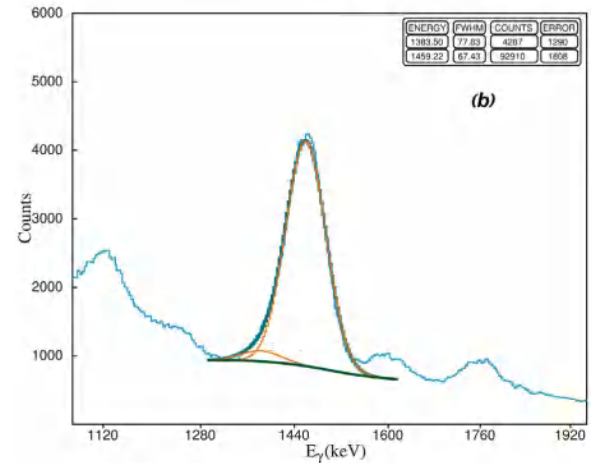
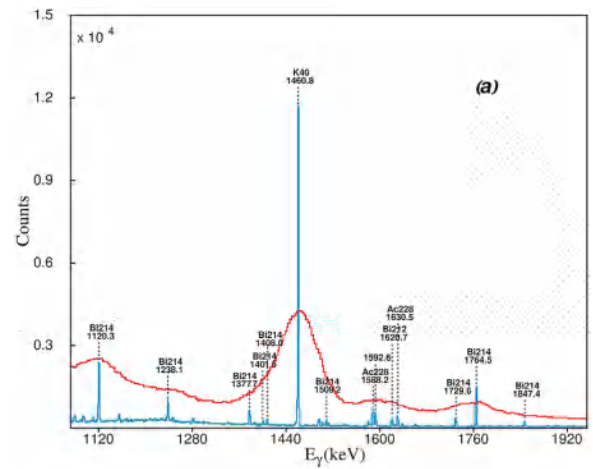


Fig. 7. (a) The HPGe and NaI spectra in the region of 1460 keV. (b) The evaluation (fitting) of the 1460.8 photo-peak.

2012) where no summing up effects are considered, the calculated activity of the interfering  $^{214}\text{Bi}$  lines is subtracted from the overall number of counts of the 1460.8 peak. In cases as the one studied here, the proposed methodology presented in this study can be used. Another way, as seen in Fig. 7b, is to de-convolute the composite peak for the group of 1377.7, 1401.5 and 1408.8 keV  $^{214}\text{Bi}$  lines, ignoring the interference of the 1509.2 keV and the summing up lines as being negligible. Both these methods gave almost identical results. It should be noted that this interference is shown in Fig. 5

### 3.1.5. Region: 1729–1847 keV

The 1729.6, 1764.5 and 1847.4 lines of  $^{214}\text{Bi}$  appear as a composite peak in the NaI spectrum (Fig. 8b). After de-convolution to separate the first two from the third (Fig. 8b), the 1729.6 + 1764.5 composite can split into its components using as before the branching ratios, the efficiency coefficients and the summing-up factors. The three  $\gamma$ -ray lines belong to  $^{214}\text{Bi}$ , so the splitting of the first two does not depend on the  $^{238}\text{U}$ -chain/ $^{232}\text{Th}$ -chain ratio.

## 3.2. Uncertainty evaluation

The activity of radionuclides in environmental samples is a function of several quantities: counting rate, detector efficiency,  $\gamma$ -ray emission probability, correction factors etc. Each of these quantities has an associated uncertainty. (IAEA, 2004; Ceccatelli et al., 2017). In this section, all the uncertainty sources, the quantification of each uncertainty component, the conversion to standard uncertainty of each uncertainty component and the proper combination of the standard uncertainties to

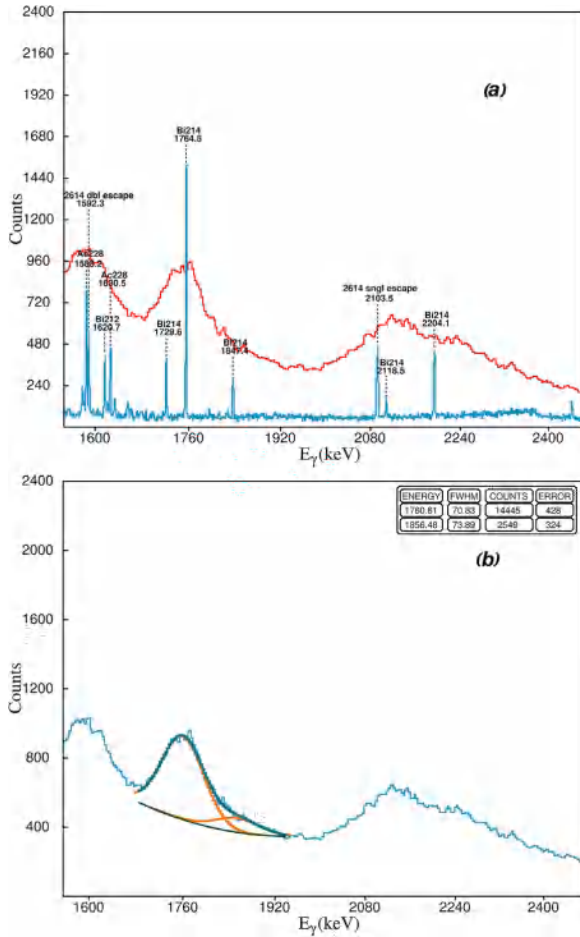


Fig. 8. (a) The HPGe and NaI spectra in the region of 1729–1847 keV. (b) Deconvolution of the composite peak.

assess the combined standard uncertainty of the activities are presented.

The net spectrum is the result of subtracting the ambient background spectrum from the sample spectrum. The net number of counts in the observed peak

$$N_{net} = N - N_{bgr} - N_{Bc} \tag{8}$$

where, N is the total number of counts in the observed peak,  $N_{bgr}$  is the ambient background and  $N_{Bc}$  is the Compton background under the peak. The statistical uncertainty in the evaluation of the peak counts is generally given by:

$$\sigma_{N_{net}} = \sqrt{\sigma_N^2 + \sigma_{N_{bgr}}^2 + \sigma_{N_{Bc}}^2} \tag{9}$$

Due to the low energy resolution, a major problem is the assessment of the Compton background,  $N_{Bc}$ , under each peak. This can be faced by taking a number of background estimates and accepting their average, modifying (increasing) accordingly the uncertainty estimate in the counts of each  $\gamma$ -line. The  $\sigma_{N_{Bc}}$  values are calculated from the distance of each individual  $N_{Bc_i}$  value from the finally accepted one  $N_{Bc}$  (Knoll, 1999a).

$$\sigma_{N_{Bc}} = \sqrt{\frac{1}{N} \sum_{i=1}^N (N_{Bc_i} - N_{Bc})^2} \tag{10}$$

When de-convoluting a composed peak, the uncertainty for each individual photo-peak results from splitting the total uncertainty of the

Table 1  
List of uncertainty sources and their contribution.

Uncertainty source	Standard uncertainty value (%)
Mass	0.04
Detector efficiency	7.5
Coincidence correction	0.8–1
BGR corrected -Net area of each of the $\gamma$ - peak	7–10
Emission probability	0.8–1

convoluted peak taking into account the net yield and the Compton background under each photo-peak. The latter is calculated from the range spanned by each photo-peak related to the expected FWHM. Then, the uncertainties obtained are further renormalized so that the square root of the sum of the squares equals the total uncertainty of the convoluted peak.

Furthermore, the uncertainty estimation  $\sigma_{C_{R\gamma}}$  of the activity  $C_{R\gamma}$  of radionuclides obtained from each individual corresponded photo-peak takes into accounts all parameters involved in the Eq. (2). For each one an uncertainty component is associated; efficiency uncertainty  $\sigma_{\epsilon_{E\gamma}}$ , uncertainty in emission probabilities  $\sigma_{I\gamma}$ , uncertainty due to sample weighing  $\sigma_m$ , uncertainty due to counting statistics (statistical uncertainty of  $N_{net}$ ), uncertainty of summing factor  $S_f$ . So the standard uncertainty  $\sigma_{C_{R\gamma}}$  is obtained from the root sum square of all the above contributing factors. In Table 1, the sources of uncertainty are listed with the percentage of their contribution. It is obvious that the main sources are the statistical uncertainty in the net counts and the uncertainty in efficiency.

If there is more than one  $\gamma$ -line from any isotope, the software used for the data analysis (SPECTRW) gives two uncertainty estimates  $\sigma_{C_R}$  and  $\sigma_{2C_R}$ . The first uncertainty is calculated from (Knoll, 1999b).

$$\sigma_{C_R} = \frac{1}{n} \sqrt{\sum_{i=1}^n \sigma_i^2} \tag{11}$$

where the symbol  $\sigma_i$  stands for the individual activity uncertainties  $\sigma_{C_{R\gamma}}$  of each  $\gamma$ -ray. The second uncertainty  $\sigma_{2C_R}$  is calculated from the distribution of the activity values, that is the distance of each point from the weighted average  $\sigma d_i = C_{Rw} - C_{R\gamma}$ . Here  $C_{Rw}$  is the weighted average of the activity for any isotope and  $C_{R\gamma}$  is the activity value for each  $\gamma$  ray. However, since the activities are not actually measured but derived values, SPECTRW modifies the distance  $\sigma d_i$  of each activity value so that  $\gamma$  lines with lower statistics contribute less in this second uncertainty derived from the distribution

$$\sigma_{2C_R} = \sqrt{\frac{\sum \left( \frac{\sigma d_i}{\sigma_{C_{R\gamma}}} \right)^2}{\sum \left( \frac{1}{\sigma_{C_{R\gamma}}} \right)^2}} \tag{12}$$

The finally adopted uncertainty value  $\sigma_{F_{R\gamma}}$  is the larger of the two. It should be noted that the uncertainties in counts in Tables 2, 3 (column 3) quoted by SPECTRW are actually calculated from the number of counts (column 2) multiplied with the relative activity uncertainty  $\frac{\sigma_{F_{R\gamma}}}{C_{R\gamma}}$ .

By adopting the larger uncertainty resulting from the two ways of uncertainty evaluation, any probable underestimation in the overall activity uncertainty in the case of multiple peaks is assumed to be avoided.

The uncertainty of  $^{238}\text{U}$  and  $^{232}\text{Th}$  activities  $u_{C_U}$  and  $u_{C_{Th}}$  are determined from the uncertainties of activities  $\sigma_{C_{Ri}}$  of the isotopes belonging to each chain, in the same way as described above using Eq. (11) and Eq. (12) and adopting the larger of the two estimates. In the present work, the overall relative activity uncertainty is about 15%, which is satisfactory for a low-resolution system.

**Table 2**

Sample Name: Giallo California, NaI STARTED ON 20 NOV 2016, ELAPSED LIVE TIME: 86400 s WEIGHT: 0.242 kg.

Energy keV	Net area counts	± Counts	Isotope	E/P %	Activity Bq/kg	± Bq/kg
1460.83	92910	9166	K40	10.67	1170	120
583.19	149819	15296	Tl208	30.36	269	28
2614.53	39608	3906	Tl208	35.64	271	27
				<u>MEAN VALUE</u>	270	20
238.63	401453	39664	Pb212	43.5	246	24
300.09	25176	3894	Pb212	3.25	240	37
				<u>MEAN VALUE</u>	244	22
609.32	87956	9691	Bi214	46.1	108	12
934.06	4976	3280	Bi214	3.16	135	90
1120.28	18793	2140	Bi214	15.00	129	15
1238.11	6055	900	Bi214	5.92	117	17
1280.96	1451	703	Bi214	1.47	117	56
1377.65	3398	430	Bi214	4.02	107	14
1385.31	656	148	Bi214	0.78	107	24
1401.50	1155	213	Bi214	1.39	107	20
1407.98	2050	305	Bi214	2.48	107	16
1729.60	2144	433	Bi214	3.05	113	23
1764.52	10953	1216	Bi214	15.90	113	13
1847.44	1922	424	Bi214	2.12	155	34
				<u>MEAN VALUE</u>	113	10
241.91	33755	8850	Pb214	7.46	121	32
295.17	65121	6686	Pb214	19.2	104	11
351.90	106381	10926	Pb214	37.1	100	10
				<u>MEAN VALUE</u>	103	12
241.00	37784	8846	Ra224	4.05	250	60
328.07	21173	5296	Ac228	3.1	226	57
338.42	75158	8252	Ac228	11.26	226	25
911.16	85846	8723	Ac228	26.60	271	28
964.64	15401	3235	Ac228	5.05	271	57
968.97	49275	5459	Ac228	16.23	271	30
				<u>MEAN VALUE</u>	252	22

#### 4. Results and discussion

The method described above in this work was used for all 20 granite samples. The emission probabilities were modified accordingly for each particular sample, depending on the ratio of  $^{238}\text{U}$  to  $^{232}\text{Th}$  decay chain, when both contribute to a composite peak.

The same method applied to one case only in the HPGe spectra, namely the 238–241 keV composite peak. Although the 238.6 keV belonging to  $^{212}\text{Pb}$  can be easily resolved, the same does not apply to the 240.00 and 241.91 keV lines belonging to  $^{224}\text{Ra}$  and  $^{214}\text{Pb}$ , respectively. As for the 186 keV composite peak, i.e. the 185.71 keV of  $^{235}\text{U}$  and 186.21 keV of  $^{226}\text{Ra}$ , the total net number of counts can be distributed 43% to  $^{235}\text{U}$  and 57% to  $^{226}\text{Ra}$ , based on the  $^{238}\text{U}$  and  $^{235}\text{U}$  relative abundance (99.3% and 0.7%), the corresponding emission probabilities and the summing factors of the two  $\gamma$ -rays.

In the present work, secular equilibrium was assumed in determining the activity of natural occurring radionuclides ( $^{238}\text{U}$  and  $^{232}\text{Th}$  chains) taking into account that, for granite samples with activity values spanning the same range as those presented here, the radon mass exhalation value reported is  $0.084 \pm 0.081 \text{ Bq kg}^{-1} \text{ h}^{-1}$  (Stoulos et al., 2003). In the case of our work (24 h acquisition time and mass of around 250 g, the radon exhalation value is negligible (0.5 Bq within the acquisition period)) compared to the measured activities.

In most cases, whether the samples are in granular form or they can be ground, secular equilibrium can be achieved by hermetically shielding them for a period of at least 30 days so that the radon can reach the equilibrium level. There are cases where extrinsic factors, such as solubility in water – important in marine research – might influence the equilibrium process. Cases where equilibrium is impossible are usually related to warfare, when depleted uranium ammunition is used.

Tables 2, 3 show in detail the analysis results in a modified format produced by SPECTRW for test sample 1 (Giallo), obtained from a NaI and an HPGe spectrometer respectively. The detailed inter-comparison is more than satisfactory, although the number of analyzed  $\gamma$ -lines in the HPGe spectrometer is approximately double when compared to that of the NaI spectrometer. The mean values shown in these tables, wherever is applicable, are the weighted average as referred previously. In the Table 2 to Table 5 the uncertainty is the combined standard uncertainty (68% confidence level). Table 4 summarizes and compares the results for the two test cases (Giallo and Caledonia). Finally, Table 5 summarizes the activity results of U, Th and K for all granite samples assuming secular equilibrium. The activity of the series U and Th are the weighted average of the activities of their individual isotopes

#### 5. Conclusions

The data analysis methodology described in this work can apply successfully in environmental research using low energy resolution detectors such as NaI. It is true that this type of analysis is more tedious and time consuming when compared to that applied using HPGe detectors. However, it is to a considerable degree reliable and meets the needs of a) small laboratories where the high cost of HPGe detectors renders them unattainable and b) data acquisition in environments, such as underwater (Tsabaris et al., 2008) where HPGe detectors cannot be used at present. Particular care should be paid in summing the individual short acquisition time spectra using the appropriate software and at the end when subtracting the ambient background spectrum from that of the sample.

The results in Table 5 show that the activities of the samples cover a wide range and are approximately in the same range as those from commercial granite samples reported in the literature (Tzortzis et al.,

**Table 3**

Sample Name: Giallo California, HPGe STARTED ON 24 NOV 2016, ELAPSED LIVE TIME: 86400 s WEIGHT: 0.242 kg.

Energy keV	Net area counts	± Counts	Isotope	E/P %	Activity Bq/kg	± Bq/kg
1460.83	37584	6247	K40	10.67	1160	190
277.35	9249	1557	Tl208	2.27	290	50
583.19	59014	9809	Tl208	30.36	268	45
763.13	909	189	Tl208	0.65	250	50
860.56	5918	989	Tl208	4.46	263	44
2614.53	19555	3253	Tl208	35.64	320	50
				<u>MEAN VALUE</u>	277	24
727.33	11123	1853	Bi212	6.64	284	47
1620.73	1235	211	Bi212	1.49	301	52
				<u>MEAN VALUE</u>	292	35
238.63	175132	29099	Pb212	43.50	255	43
300.09	12000	2006	Pb212	3.25	282	47
				<u>MEAN VALUE</u>	267	32
609.32	38726	6438	Bi214	46.10	121	20
665.45	1326	258	Bi214	1.56	133	26
768.36	3512	597	Bi214	4.88	129	22
806.17	878	175	Bi214	1.23	133	27
934.06	2042	355	Bi214	3.16	139	24
1120.28	8043	1342	Bi214	15.00	137	23
1238.11	3146	532	Bi214	5.92	150	25
1280.96	768	148	Bi214	1.47	150	30
1377.65	1767	299	Bi214	4.02	137	23
1385.31	331	76	Bi214	0.78	133	31
1401.50	710	137	Bi214	1.39	161	31
1407.98	1156	202	Bi214	2.48	148	26
1509.19	900	159	Bi214	2.19	139	25
1661.28	441	84	Bi214	1.15	143	27
1729.60	966	164	Bi214	3.05	122	21
1764.52	5314	886	Bi214	15.90	132	22
1847.44	703	122	Bi214	2.12	137	24
				<u>MEAN VALUE</u>	136	10
241.91	15796	2638	Pb214	7.46	135	23
295.17	29499	4906	Pb214	19.20	116	20
351.90	49054	8154	Pb214	37.10	116	20
				<u>MEAN VALUE</u>	121	12
241.00	16214	2287	Ra224	4.05	255	36
186.21	8481	1431	Ra226	3.51	127	22
209.39	17461	2913	Ac228	3.81	262	44
270.26	15721	2623	Ac228	3.44	319	53
328.07	11003	1840	Ac228	3.10	292	50
338.42	34943	5810	Ac228	11.26	262	44
463.10	11485	1916	Ac228	4.50	285	48
794.79	6918	1157	Ac228	4.34	293	50
835.60	2544	436	Ac228	1.80	273	47
911.16	33441	5559	Ac228	26.60	263	44
964.64	6761	1134	Ac228	5.05	296	50
968.97	19865	3319	Ac228	16.23	272	45
1588.23	2557	429	Ac228	3.26	279	47
1630.47	1396	237	Ac228	1.53	333	57
				<u>MEAN VALUE</u>	283	20
185.71	6564	1121	U235	57.20	6.0	1.0



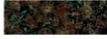
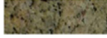



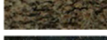
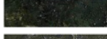
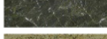


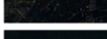
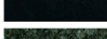
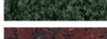
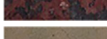
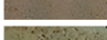
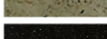


**Table 4**

HPGe and NaI results activity comparison.

Isotope	Granite: Giallo California		Granite: New Caledonia	
	HPGe Activity (Bq/kg)	NaI Activity (Bq/kg)	HPGe Activity (Bq/kg)	NaI Activity (Bq/kg)
K40	1160 ± 190	1173 ± 120	1220 ± 200	1180 ± 120
Tl208	277 ± 24	270 ± 20	84 ± 7	84 ± 5
Bi212	290 ± 40	–	80 ± 11	–
Pb212	270 ± 30	240 ± 22	80 ± 10	75 ± 8
Bi214	140 ± 10	110 ± 10	11 ± 3	9.0 ± 2.0
Pb214	120 ± 12	100 ± 12	9.0 ± 0.9	9.0 ± 1.1
Ra224	260 ± 40	250 ± 60	70 ± 13	75 ± 7
Ra226	130 ± 20	–	8 ± 5	–
Ac228	280 ± 20	250 ± 22	80 ± 5	83 ± 9
U235	6.0 ± 0.9	–	0.4 ± 0.3	–



**Table 5**  
Activity results - Summary.

Sample name	Place of origin	Density g/cm <sup>3</sup>	Picture	Activity Bq/kg		
				<sup>40</sup> K	<sup>238</sup> U chain	<sup>232</sup> Th chain
Balmoral	Norway	2.541		1380 ± 120	76 ± 9	190 ± 14
Café Imperial	Brazil	2.642		1860 ± 180	17 ± 3	40 ± 3
Carmen Red	Finland	2.588		1380 ± 140	108 ± 6	240 ± 11
Cecilia	Brazil	2.571		1030 ± 100	24 ± 5	40 ± 4
Colombo	India	2.596		700 ± 60	19.3 ± 2.2	50 ± 5
Crema Azul Bahia	Brazil	2.616		1210 ± 110	29 ± 4	70 ± 7
Emerald Pearl	Norway	2.632		970 ± 90	40 ± 3	50 ± 5
Giallo California	Brazil	2.535		1170 ± 120	109 ± 8	260 ± 17
Green Uba Tuba	Brazil	2.676		770 ± 70	18 ± 3	48 ± 4
Ital Green	Italy	2.592		440 ± 40	12.2 ± 2.1	33 ± 3
Ivory Brown	India	2.610		990 ± 100	90 ± 6	8.1 ± 2.2
Juparana	India	2.636		1450 ± 130	32 ± 5	130 ± 11
Labrador	Brazil	2.588		1610 ± 140	16.0 ± 1.2	19.0 ± 2.3
Nero Africa	S. Africa	2.825		120 ± 12	7.9 ± 1.1	6.9 ± 1.2
New Caledonia	Brazil	2.572		1180 ± 120	9.1 ± 2.0	80 ± 4
Red Africa	S. Africa	2.522		1260 ± 120	46 ± 7	78 ± 5
Rosa Quartzite	Brazil	2.457		160 ± 14	8.1 ± 0.9	7.9 ± 1.1
Shivacasi	India	2.503		1060 ± 90	38.8 ± 2.3	7.1 ± 2.1
Star Galaxy	India	2.861		190 ± 20	8.0 ± 1.1	9.2 ± 1.2
Zimbabwe	Zimbabwe	2.993		330 ± 30	13.4 ± 2.2	25.2 ± 2.1

2003; Pavlidou et al., 2006), and found below or very near the accepted safety levels. An additional point is that in all cases <sup>40</sup>K has the highest activity. As for the <sup>238</sup>U-chain and <sup>232</sup>Th-chain activities, in general, black or gray granites tend to exhibit smaller values than those with red, yellow or green colors. As an extra comparison, white Pendelikon marble (similar to the one used for Parthenon) showed no detectable activity whatsoever when tested with the NaI spectrometer.

The activity alone is not a measure of the degree of safety risk, which depends on additional factors. The total energy radiated in the form of  $\gamma$ -rays and eventually absorbed by a human is a key factor for the external exposure. It depends on the average number of  $\gamma$ -rays in cascade, the range of  $\gamma$ -ray energies, the number of radioactive isotopes in a decay chain and not the least, the area covered with the radiating material that surrounds those exposed to it. Although the issue of radiation absorbed dose is beyond the scope of this work, when using NaI detectors a useful picture could be drawn by integrating the whole net spectrum recorded from a sample in a wide energy range (e.g. up to 3.5 MeV) and doing the same for the ambient background. The ratio of the two values could be indicative of the relative intensity of the radioactivity of that sample.

#### Acknowledgments

The authors would like to thank manufacturers, Mr P. Tountas (Thivon 273) and Mr. M. Anogianakis, (Thivon 271), Aegaleo Greece, for supplying gratis the granite samples.

The  $\gamma$ -ray spectrometry system was purchased through the financing program “PEP ATTIKIS” 2007–2013.

#### References

- Anjos, R.M., Okuno, E., Gomes, P.R.S., Veiga, R., Estellita, L., Mangia, L., Uzeda, D., Soares, T., Fature, A., Brage, J.A.P., 2003. Radioecology teaching: evaluation of the background radiation levels from areas with high concentrations of radionuclides in soil. *Eur. J. Phys.* 25, 133–144.
- Bezuidenhout, J., 2013. Measuring naturally occurring uranium in soil and minerals by analysing the 352 keV gamma-ray peak of <sup>214</sup>Pb using a NaI(Tl)-detector. *Appl. Radiat. Isot.* 80, 1–6.
- Ceccatelli, M., Dybdal, A., Fajgelj, A., Pitois, A., 2017. Calculation spreadsheet for uncertainty estimation of measurement results in gamma-ray spectrometry and its validation for quality assurance purpose. *Appl. Radiat. Isot.* 124, 7–15.
- Chiozzi, P., Pasquale, V., Verdoya, M., De Felice, P., 2003. Practical applicability of field  $\gamma$ -ray scintillation spectrometry in geophysical surveys. *Appl. Radiat. Isot.* 53, 215–220.
- Cinelli, G., Tositti, L., Mostacci, D., Bare, J., 2016. Calibration with MCNP of NaI detector for the determination of natural radioactivity levels in the field. *J. Environ. Radioact.* 155–156, 31–37.
- Firestone, R.B., 1996. Table of isotopes Vers. 1.0. In: Firestone, R.B., Shirley, V.S. (Eds.), *Lawrence Berkeley Laboratory*. Published by John Wiley & Sons, Inc. (ISBN 0471-14918-7).
- IAEA, 2003. (IAEA-TECDOC; Vol. 1363): Guidelines for Radioelement Mapping Using Gamma Ray Spectrometry Data (Vienna: International Atomic Energy Agency).
- IAEA, 2004. (IAEA-TECDOC-1401): Quantifying uncertainty in nuclear analytical measurement Dvlete, C., Povinec, P.P., Quantification of uncertainty in gamma-spectrometric analysis of environmental samples (Vienna: International Atomic Energy Agency).
- IAEA, 2016. Revision: Safety Glossary Terminology used in Nuclear Safety and Radiation Protection (Vienna: International Atomic Energy Agency).
- IUPAC, 1996. 68, 957. Glossary of Terms in Quantities and Units in Clinical Chemistry (IUPAC-IFCC Recommendations 1996), doi:10.1351/pac199668040957 (<http://goldbook.iupac.org/html/S/S05790.html>).
- Kalfas, C.A., Axiotis, M., Tsabaris, C., 2016. SPECTRW: a software package for nuclear and atomic spectroscopy. *Nucl. Instrum. Methods A* 830, 265–274.
- Knoll, F.G., 1999a. *Radiation Detection and Measurement*, Third edition. John Wiley & Sons, Inc, pp. 69 (ISBN 0-471-07338-5).
- Knoll, F.G., 1999b. *Radiation Detection and Measurement*, Third edition. John Wiley &

- Sons, Inc., pp. 91–92 (ISBN 0-471-07338-5).
- Pavlidou, S., Koroneos, A., Papastefanou, C., Christofides, G., Stoulos, S., Vavelides, M., 2006. Natural radioactivity of granites used as building materials. *J. Environ. Radioact.* 89, 48–60.
- Pilakouta, M., Savidou, A., Vasileiadou, S., 2017. A laboratory activity for teaching natural radioactivity. *Eur. J. Phys.* 38, 015801.
- Stoulos, S., Manolopoulou, M., Papastefanou, C., 2003. Assessment of natural radiation exposure and radon exhalation from building materials in Greece. *J. Environ. Radioact.* 69, 225–240.
- Tsabarlis, C., Eleftheriou, G., Kapsimalis, V., Anagnostou, C., Vlastou, R., Durmishi, C., Kedhi, M., Kalfas, C.A., 2007. Radioactivity levels of recent sediments in the Butrint Lagoon and the adjacent coast of Albania. *Appl. Radiat. Isot.* 65, 445–453.
- Tsabarlis, C., Bagatelas, C., Dakladas, Th, Papadopoulos, C.T., Vlastou, R., Chronis, G.T., 2008. An autonomous in situ detection system for radioactivity measurements in the marine environment. *Appl. Radiat. Isot.* 66, 1419–1426.
- Tsabarlis, C., Patiris, D.L., Karageorgis, A.P., Eleftheriou, G., Papadopoulos, V.P., Georgopoulos, D., Papathanassiou, E., Povinec, P.P., 2012. In-situ radionuclide characterization of a submarine groundwater discharge site at Kalogria Bay, Stoupa, Greece. *J. Environ. Radioact.* 108, 50–59.
- Tzortzis, M., Tsertos, H., Christofides, S., Christodoulides, G., 2003. Gamma radiation measurements and dose rates in commercially-used natural tiling rocks (granites). *J. Environ. Radioact.* 70, 223–235.
- Vidmar, T., 2005. EFFTRAN - A Monte Carlo efficiency transfer code for  $\gamma$ -ray spectrometry. *Nucl. Instrum. Methods A* 550, 603–608.